Electronic Supplementary Material (ESI) for Journal of Materials Chemistry A.

Supporting Information for

Graphene-MoS$_2$ Vertically Anchored on MXene-Derived Accordion-like TiO$_2$/C Skeleton: An Ultrastable HER Catalyst

Jian Li, Zi Wen, Zhen Xin Hui, Zhi Wen Chen, Chun Cheng Yang,* Qing Jiang*

Key Laboratory of Automobile Materials (Jilin University), Ministry of Education, and School of Materials Science and Engineering, Jilin University, Changchun 130022, China

* *Corresponding authors. Tel.: +86-431-85095371; Fax: +86-431-85095876; E-mails: ccyang@jlu.edu.cn (C. C. Yang); jiangq@jlu.edu.cn (Q. Jiang).*

† Electronic Supplementary Information (ESI) available. See DOI: 10.1039/x0xx00000x

Materials and methods

Synthesis of T_2C MXene: The Ti_2AlC powder was sieved below 25 μm with a 500-mesh sieve before use. For preparing 2D layered Ti_2C MXene, 3 g Ti_2AlC was added into 40 ml 10% HF with mechanical stirring for 12 h. The obtained powder was washed with deionized water and ethanol for several times and dried at 60 ºC in a vacuum oven overnight.

Synthesis of rGO-MoS_2/Acc-TiO_2/C: Graphene oxide (GO) was synthesized using a modified Hummers' method.[1,2] For the *in-situ* synthesis of rGO-MoS_2/Acc-TiO_2/C, 40 mg ammonium molybdate tetrahydrate, 0.6 g thiourea and 25 mg Ti_2C MXene were dissolved in 10 ml ultrapure water to form a uniform solution. 0.7 ml GO (5 mg ml^{-1}) was then added into the solution. The mixture solution was transferred into a Teflon-lined stainless-steel autoclave and heated to 160 ºC for 24 h. The resulting powder was cleaned by centrifugation with deionized water, and dried at 60 ºC in a vacuum oven overnight.

Synthesis of MoS_2/Acc-TiO_2/C, rGO-MoS_2 and MoS_2: MoS_2/Acc-TiO_2/C and rGO-MoS_2 were prepared with the same method as rGO-MoS_2/Acc-TiO_2/C except for the addition of GO and Ti_2C MXene, respectively, before the hydrothermal reaction. MoS_2 was synthesized using the same means as MoS_2/Acc-TiO_2/C without the addition of Ti_2C MXene when preparing the precursor solution.

Synthesis of TiO_2/C: For the fabrication of TiO_2/C, 25 mg as-prepared Ti_2C was dissolved into 10 ml ultrapure water to form a mixture solution, which was then hydrothermally heated to 160 ºC for 24 h.

Material Characterization: X-ray diffraction (XRD) patterns were obtained using a D/max2500pc diffractometer with Cu $K\alpha$ radiation ($\lambda = 0.15406$ nm). Raman analysis was performed on a micro-Raman spectrometer (Renishaw) through a 532-nm wavelength laser source. Specific area and pore size distribution were recorded by nitrogen (N_2) adsorption-desorption isotherms with a Micromeritics ASAP 2020 analyzer. A field-emission scanning electron microscope (FESEM, JSM-6700F, JEOL, 15 keV) and a transmission electron microscope (TEM, JEM-2100F, JEOL, 200 keV) were employed to investigate the surface morphology and microstructure. X-ray photoelectron spectroscopy (XPS) measurement was carried out through a monochromatic Al-K_{α} (1486.6 eV) source on an ESCALAB 250Xi spectrometer (Thermo Fisher Scientific, US).

Electrochemical Measurements: The electrochemical measurements were carried out on an Ivium-n-Stat electrochemical workstation in 0.5 M H_2SO_4 at room temperature. A standard three-electrode system was used with a catalyst covered glassy carbon rotating disk (5 mm in diameter) electrode (RDE, Pine Research Instrumentation) as the working electrode, a graphite rod as the counter electrode, and a saturated calomel electrode (Hg/Hg_2Cl_2, SCE) as the reference electrode. To prepare the catalyst ink, 2.5 mg catalyst powders were dispersed into 0.5 ml mixture of water-isopropanol solution (4:1, v/v) containing 50 μl 5 wt% Nafion solution through sonication for 30 min. 15 μl as-prepared catalyst ink was then spread on the surface of a polished glassy carbon electrode (GCE) and dried at room temperature. Linear sweep voltammetry (LSV) was carried out with a rotation rate of 2025 rpm at a scan rate of 5 mV s^{-1}. Electrochemical impedance test was measured in the frequency range from 100 kHz to 0.1 Hz at an overpotential of 250 mV *vs*. the reversible hydrogen evolution (RHE). Cyclic voltammetry (CV) measurements were conducted under an overpotential range from -200 to 100 mV (*vs*. RHE) for pristine MoS_2, MoS_2/Acc-TiO_2/C, rGO-MoS_2 and rGO-MoS_2/Acc-TiO_2/C at a sweep rate of 50 mV s^{-1} and -50 to 100 mV (*vs*. RHE) for Pt/C at a sweep rate of 100 mV s^{-1}, respectively.

Chronoamperometry was carried out at a current density of -10 mA cm^{-2} for 200,000 s. All the measured potentials were converted to the potentials versus RHE by E_{RHE} = E_{SCE} + 0.059 pH + E_{SCE}^{0}, where E_{RHE}, E_{SCE} and E_{SCE}^{0} denote the reversible hydrogen evolution potential, the measured potential and the saturated calomel electrode potential, respectively. N_2 gas flow was carried out through the electrolyte for 30 min to purify the solution before the electrochemical measurements. The Faradic efficiency of hydrogen production was measured at -0.5 V (*vs.* RHE) with a gas chromatograph (GC-2014). CO_2 was introduced into the electrolyte at a rate of 40 ml min^{-1} as a carrier gas and the H_2 quantification was detected every 10 min through a thermal conductivity detector (TCD).

Computational Details: For catalyst design in this research, we carried out the spin-unrestricted DFT calculations in the Dmol^3 code.[3,4] A generalized gradient approximation (GGA) with Perdew-Burke-Ernzerhof correlation (PBE) was utilized to describe the effects of exchange-correlation.[5] Core electrons are substituted by a single effective potential through DFT semi-core pseudo potentials (DSPPs) considering the relativistic effects.[6] Furthermore, the basis set was double numerical plus polarization (DNP) with high quality for the orbital cutoff of 4.9 Å. To get geometrically optimized structures, the convergence criteria were 2.0×10^{-3} Ha Å^{-1} for the energy gradient, 5.0×10^{-3} Ha Å^{-1} for the displacement, and 1.0×10^{-5} Ha for the energy change. In this simulation, the actual spacing of k-point sampling was set around 0.03 Å^{-1} for three directions and three-dimensional periodic boundary conditions were taken.

For the calculation of transition states, we applied the climbing image nudges elastic band method (CI-NEB) as implemented in the Vienna ab-initio simulation package (VASP).[7] The energy cutoff for the plane-wave basis was set at 400 eV. The convergences of energy and interatomic forces were 10^{-6} eV and 0.05 eV Å^{-1}, respectively. Among the Heyrovsky and Tafel reactions mechanisms, the proton was simulated by two H_2O molecules with one H^+ ($H_5O_2^+$), which has been proved to be successful by previous works.[8,Ref. 27 of the text]

In this work, we considered both vertical and parallel MoS_2 nanosheets on TiO_2 substrate. The corresponding adhesion energy value (W_{ad}) between MoS_2 and TiO_2 was calculated by

$$W_{\mathrm{ad}} = \frac{E_{\mathrm{MoS_2}} + E_{\mathrm{TiO_2}} - E_{\mathrm{MoS_2\text{-}TiO_2}}}{\mathrm{S}} \tag{1}$$

where $E_{\mathrm{MoS_2}}$, $E_{\mathrm{TiO_2}}$, $E_{\mathrm{MoS_2\text{-}TiO_2}}$ denoted the total energy of MoS_2, TiO_2, and MoS_2-TiO_2 composites, respectively, while S represented the interfacial area between MoS_2 and TiO_2.[9]

Supplementary Figures

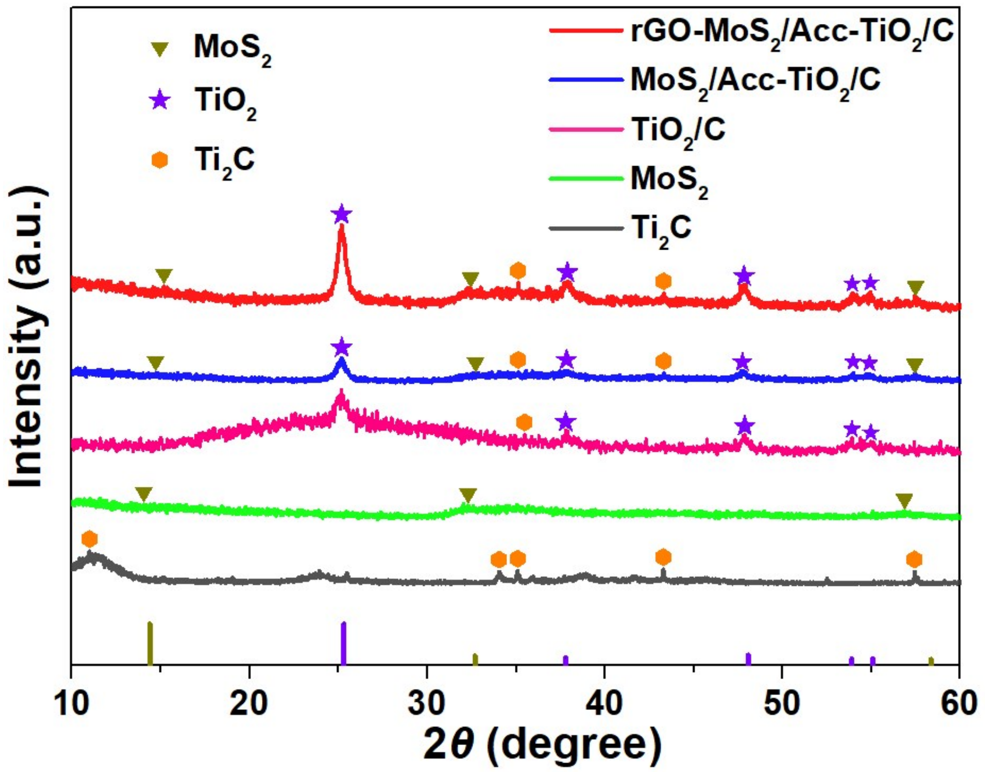

Fig. S1 XRD patterns of Ti_2C, MoS_2, TiO_2/C, MoS_2/Acc-TiO_2/C and rGO-MoS_2/Acc-TiO_2/C.

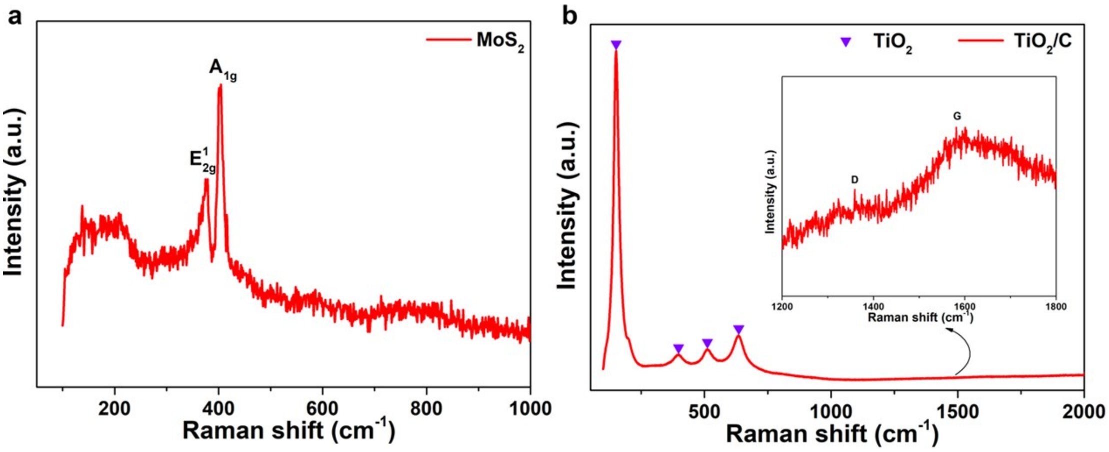

Fig. S2 Raman analysis of comparative samples. (a) Raman spectrum of pristine MoS$_2$. (b) Raman spectrum of bare TiO$_2$/C. The inset is the local spectrum from 1200 to 1800 cm^{-1}.

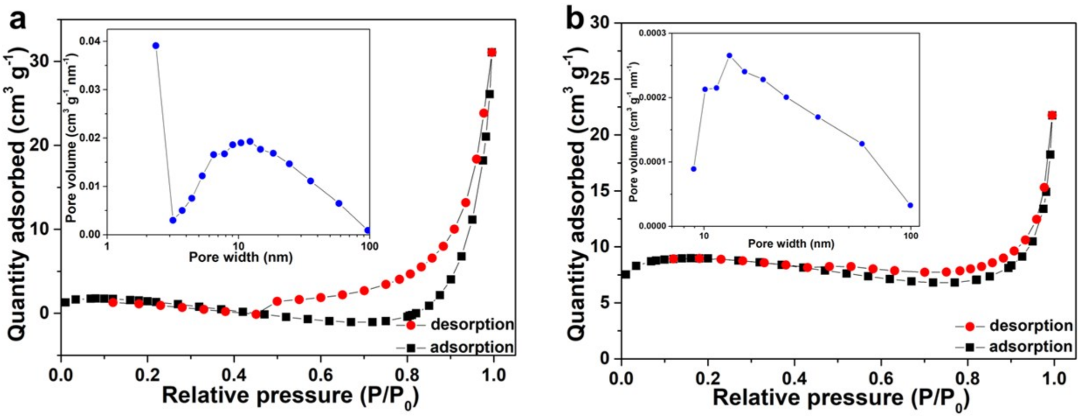

Fig. S3 The specific surface area and pore size distribution analysis of comparative samples. N_2 adsorption/desorption isotherms and pore size distribution (the inset) of (a) bare MoS_2 and (b) Ti_2C MXene.

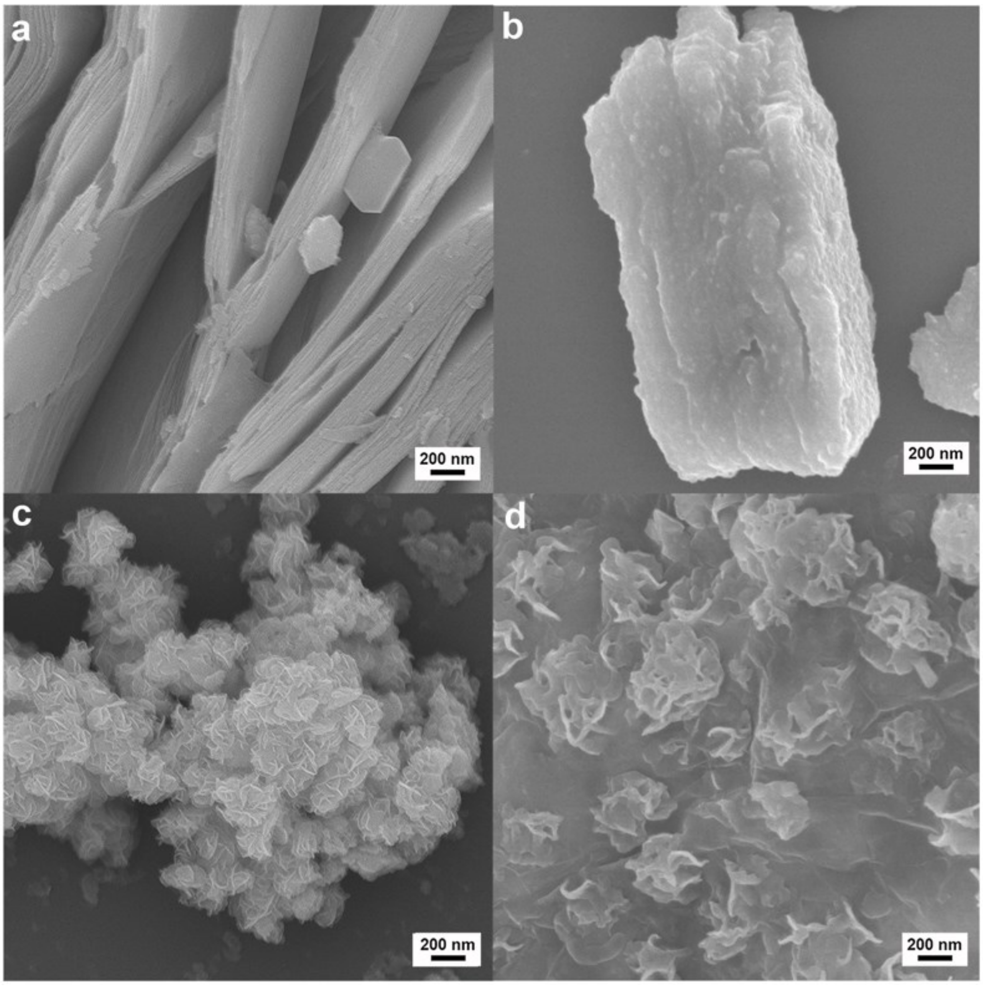

Fig. S4 Morphology characterization of comparative samples. SEM images of (a) Ti_2C MXene, (b) bare TiO_2/C, (c) pristine MoS_2, and (d) rGO-MoS_2.

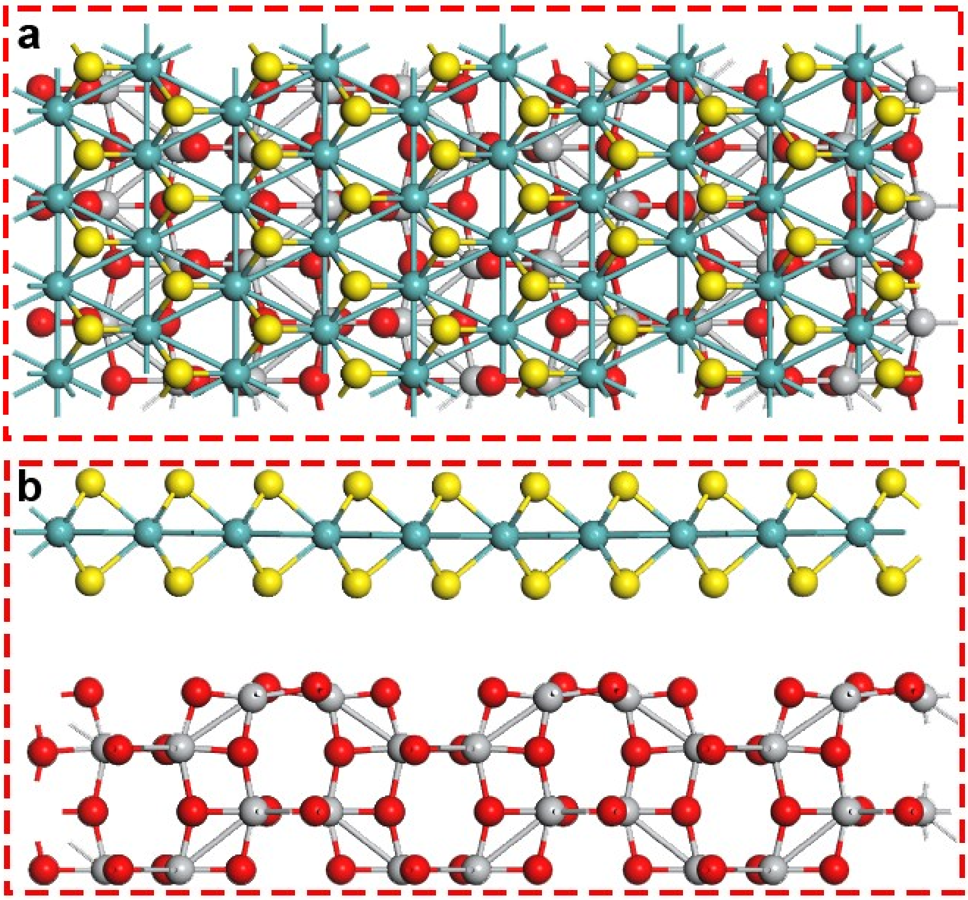

Fig. S5 Atomic structure of MoS_2/TiO_2. (a) Top view and (b) side view of atomic structures of MoS_2/TiO_2, where MoS_2 grows parallel to TiO_2.

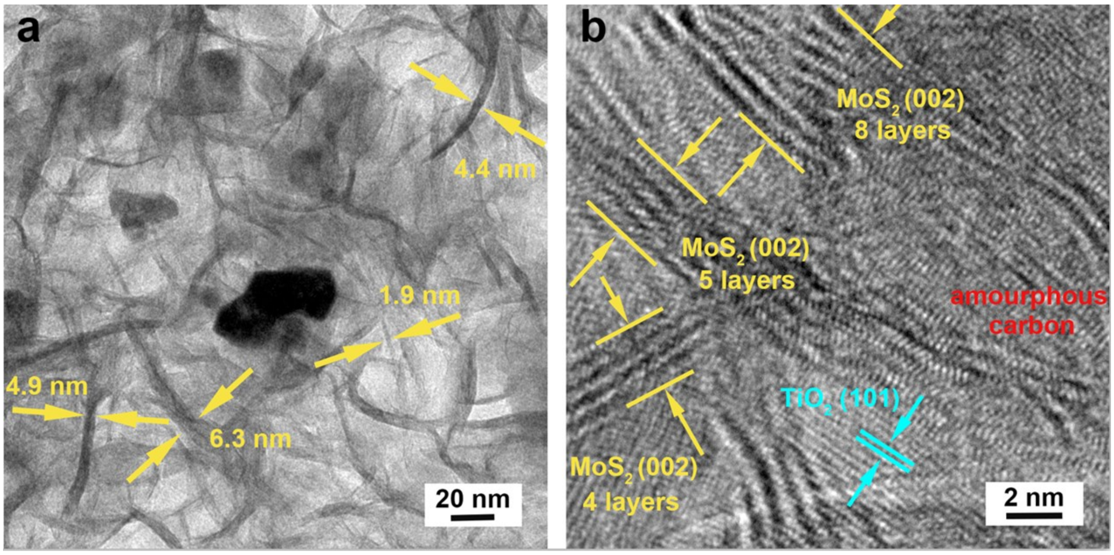

Fig. S6 Identification of the MoS_2 thickness of rGO-MoS_2/Acc-TiO_2/C. (a) TEM and (b) HRTEM images of rGO-MoS_2/Acc-TiO_2/C.

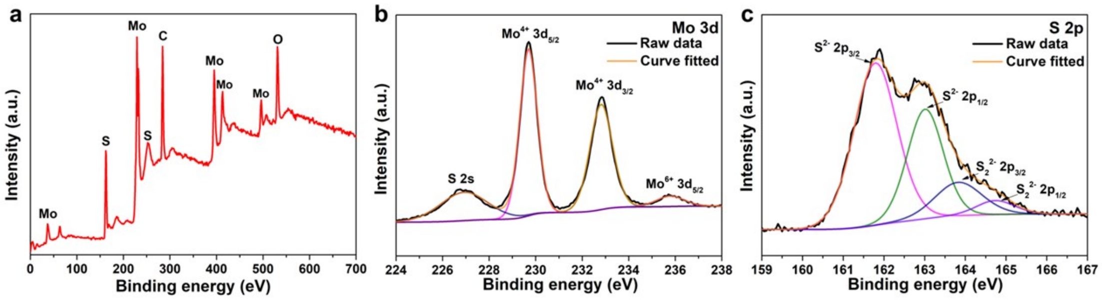

Fig. S7 XPS analysis of bare MoS_2. (a) XPS survey spectrum of bare MoS_2. (b) and (c) High-resolution XPS spectra of Mo 3d and S 2p, respectively.

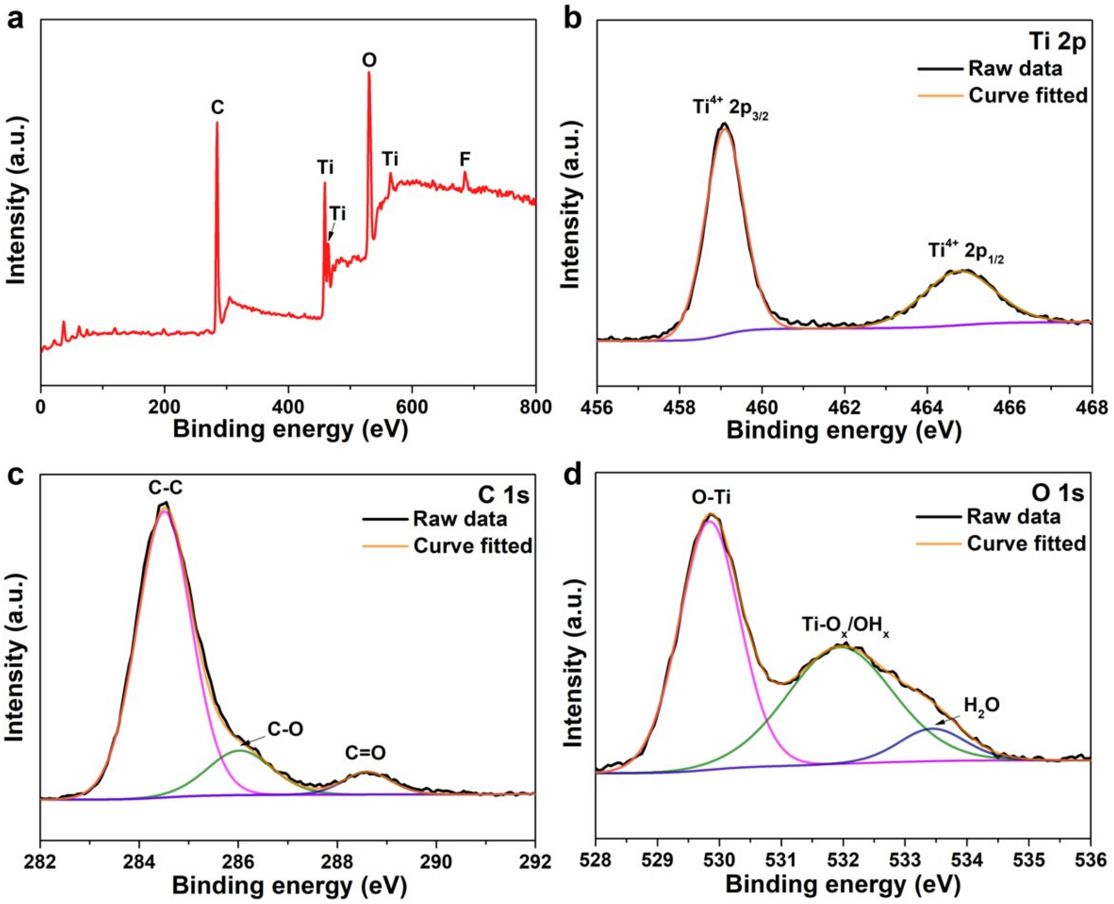

Fig. S8 XPS analysis of bare Ti_2O/C. (a) XPS survey spectrum of Ti_2O/C. (b)-(d) High-resolution XPS spectra of Ti 2p, C 1s and O 1s, respectively.

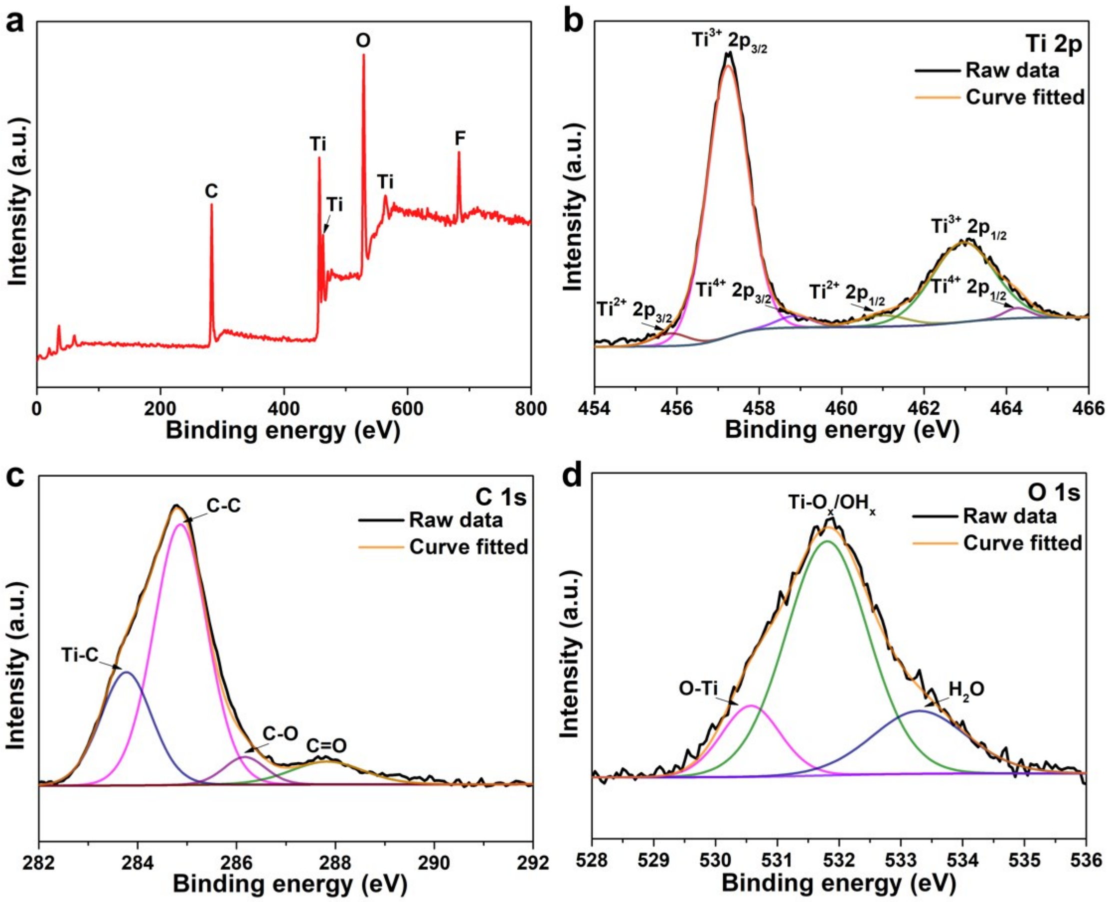

Fig. S9 XPS analysis of Ti_2C MXene. (a) XPS survey spectrum of Ti_2C MXene. (b)-(d) High-resolution XPS spectra of Ti 2p, C 1s and O 1s, respectively.

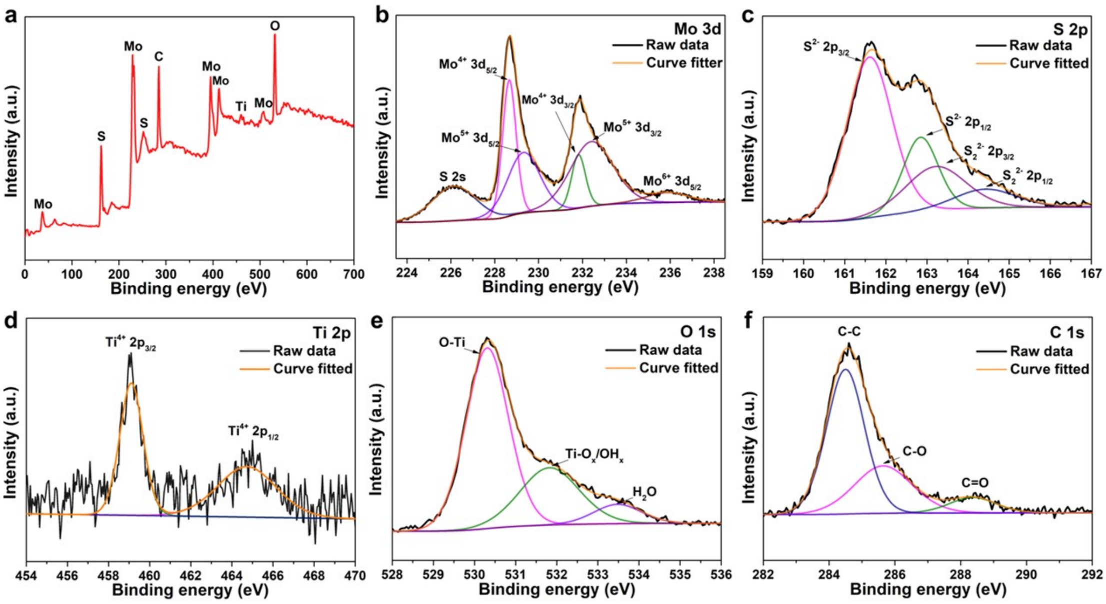

Fig. S10 XPS analysis of MoS_2/Acc-TiO_2/C. (a) XPS survey spectrum of MoS_2/Acc-TiO_2/C. (b)-(f) High-resolution XPS spectra of Mo 3d, S 2p, Ti 2p, O 1s and C 1s of MoS_2/Acc-TiO_2/C, respectively.

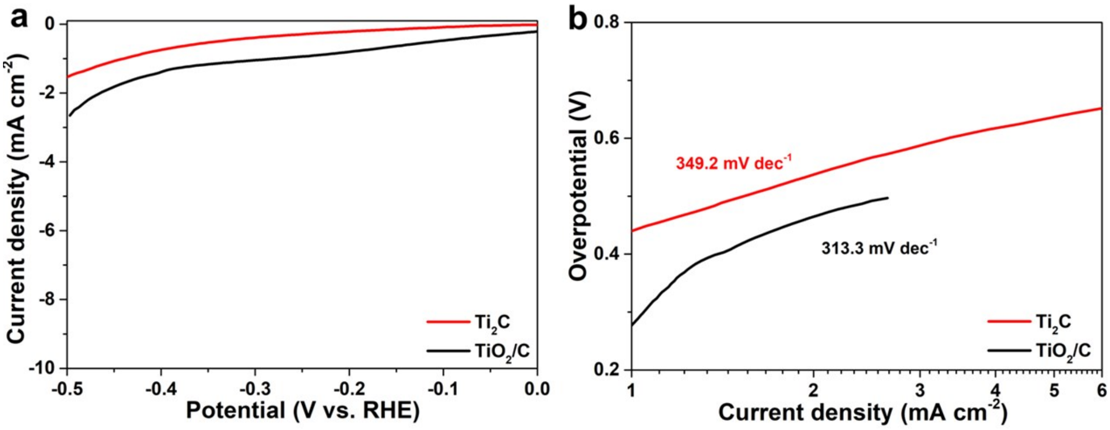

Fig. S11 HER performances of the substrate. (a) Polarization curves and (b) Tafel plots of Ti_2C and TiO_2/C.

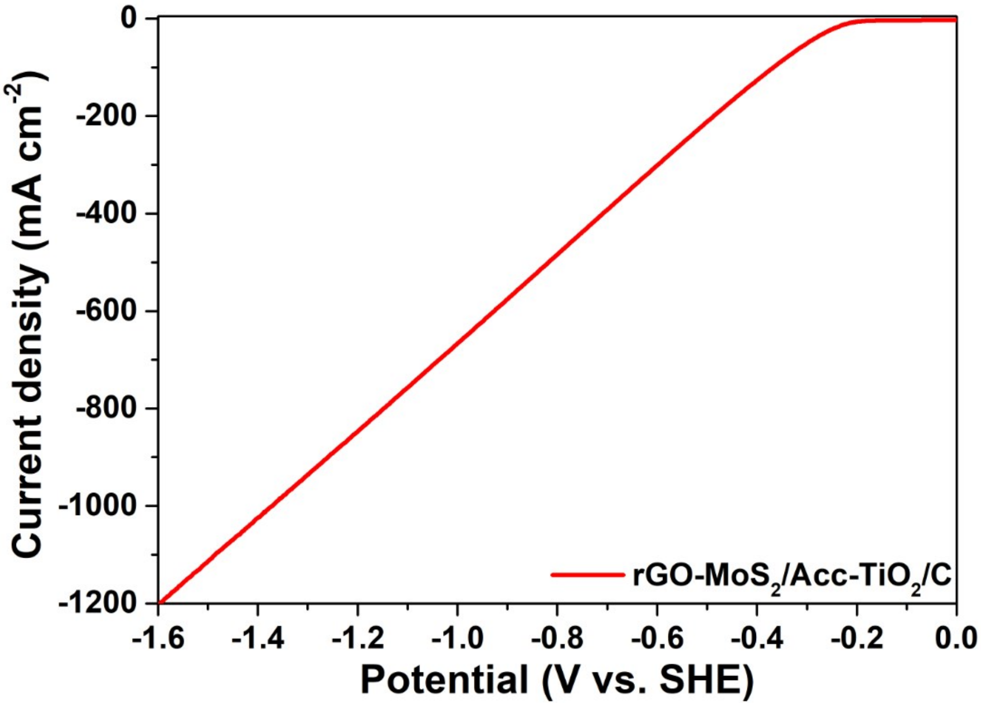

Fig. S12 Polarization curve of rGO-MoS_2/Acc-TiO_2/C at a potential range from -1.6 to 0 V *vs*. the standard hydrogen electrode (SHE).

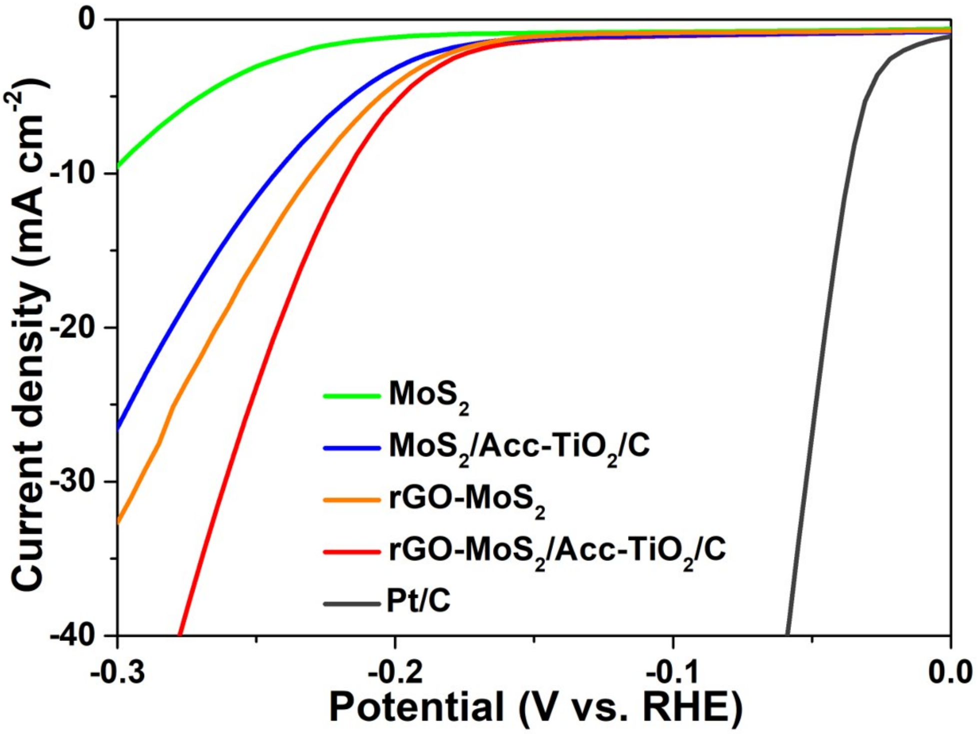

Fig. S13 Polarization curves of bare MoS$_2$, MoS$_2$/Acc-TiO$_2$/C, rGO-MoS$_2$, rGO-MoS$_2$/Acc-TiO$_2$/C and commercial Pt/C without *IR*-compensation.

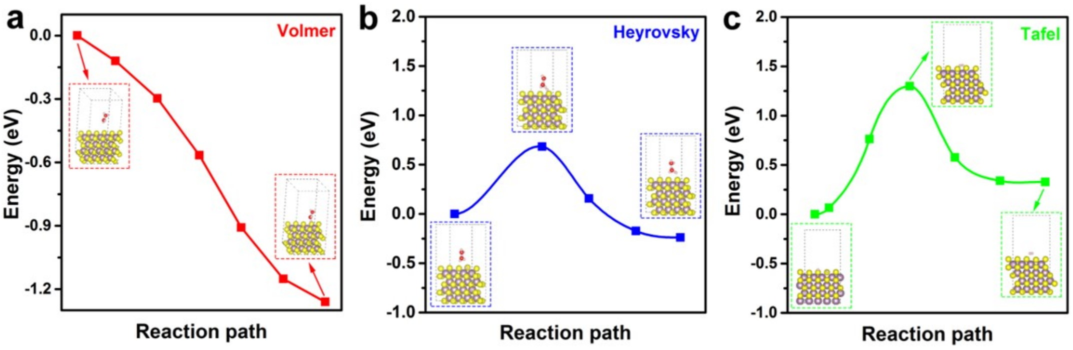

Fig. S14 Reaction paths of (a) Volmer, (b) Heyrovsky, and (c) Tafel reactions of HER on MoS_2 edges.

Table S1. Summary of the specific surface area, pore size distribution and catalytic activity of Ti_2C, MoS_2 and rGO-MoS_2/Acc-TiO_2/C.

Catalyst	Specific surface area (m^2 g^{-1})	Pore size distribution (nm)	η at 10 mA cm^{-2} (mV)
Ti_2C	2.4	mainly 10 ~ 25	---
MoS_2	25.0	mainly 7 ~ 25	289
rGO-MoS_2/Acc-TiO_2/C	45.3	mainly ~ 4	207

Table S2. Summary of the bonding forms of different elements and the corresponding catalytic activity of MoS_2, MoS_2/Acc-TiO_2/C, rGO-MoS_2/Acc-TiO_2/C, rGO-MoS_2/Acc-TiO_2/C after the stability test, Ti_2O/C and Ti_2C.

Catalyst	The valence of Ti	The ratio of O-Ti bond to O-containing bonds	The existence of Mo^{5+}	The ratio of S_2^{2-} to S-containing bonds	η at 10 mA cm^{-2} (mV)
MoS_2	---	---	does not exist	16.2%	289
MoS_2/Acc-TiO_2/C	Ti^{4+}	64.1%	exists	27.2%	239
rGO-MoS_2/Acc-TiO_2/C	Ti^{4+}	51.3%	exists	24.8%	207
rGO-MoS_2/Acc-TiO_2/C after the stability test	Ti^{4+}	8.9%	exists	17.1%	218
Ti_2O/C	Ti^{4+}	51.0%	---	---	---
Ti_2C	90.5% Ti^{3+}; 5.7% Ti^{2+}; 3.8% Ti^{4+}	14.2%	---	---	---

Notes and references

1 D. C. Marcano, D. V. Kosynkin, J. M. Berlin, A. Sinitskii, Z. Z. Sun, A. Slesarev, L. B. Alemany, W. Lu and J. M. Tour, *ACS Nano*, 2010, **4**, 4806-4814.

2 M. M. Li, C. C. Yang, L. X. Chen and Q. Jiang, *Electrochim. Acta*, 2016, **200**, 59-65.

3 B. Delley, *J. Chem. Phys.*, 2000, **113**, 7756-7764.

4 B. Delley, *J. Chem. Phys.*, 1990, **92**, 508-517.

5 J. P. Perdew, K. Burke and M. Ernzerhof, *Phys. Rev. Lett.*, 1996, **77**, 3865-3868.

6 B. Delley, *Phys. Rev. B*, 2002, **66**, 155125.

7 G. Kresse and J. Furthmüller, *Comp. Mater. Sci.*, 1996, **6**, 15-50.

8 G. P. Gao, Q. Sun and A. Du, *J. Phys. Chem. C,* 2016, **120**, 16761-16766.

9 A. Tkatchenko and M. Scheffler, *Phys. Rev. Lett.*, 2009, **102**, 073005.